Journal of
Micro/Nanolithography,
MEMS, and MOEMS

Nanolithography.SPIEDigitalLibrary.org

Extreme UV secondary electron yield measurements of Ru, Sn, and Hf oxide thin films

Jacobus M. Sturm
Feng Liu
Erik Darlatt
Michael Kolbe
Antonius A. I. Aarnink
Christopher J. Lee
Fred Bijkerk

SPIE.

Jacobus M. Sturm, Feng Liu, Erik Darlatt, Michael Kolbe, Antonius A. I. Aarnink, Christopher J. Lee, Fred Bijkerk, "Extreme UV secondary electron yield measurements of Ru, Sn, and Hf oxide thin films," *J. Micro/Nanolith. MEMS MOEMS* **18**(3), 033501 (2019), doi: 10.1117/1.JMM.18.3.033501.

Downloaded From: https://www.spiedigitallibrary.org/journals/Journal-of-Micro/Nanolithography,-MEMS,-and-MOEMS on 01 Oct 2019
Terms of Use: https://www.spiedigitallibrary.org/terms-of-use

J. Micro/Nanolith. MEMS MOEMS 18(3), 033501 (Jul–Sep 2019)

Extreme UV secondary electron yield measurements of Ru, Sn, and Hf oxide thin films

Jacobus M. Sturm,[a,*] Feng Liu,[a] Erik Darlatt,[b] Michael Kolbe,[b] Antonius A. I. Aarnink,[c] Christopher J. Lee,[a,†] and Fred Bijkerk[a]
[a]University of Twente, MESA+ Institute, Industrial Focus Group XUV Optics, Enschede, The Netherlands
[b]Physikalisch-Technische Bundesanstalt, Berlin, Germany
[c]University of Twente, MESA+ Institute, Integrated Devices and Systems Group, Enschede, The Netherlands

Abstract

Background: The secondary electron yield (SEY) of materials is important for topics as nanoparticle photoresists and extreme ultraviolet (EUV) optics contamination.

Aim: Experimentally measure SEY and secondary electron energy distributions for Ru, Sn, and Hf oxide.

Approach: The SEY and energy distribution resulting from 65 to 112 eV EUV radiation are measured for thin-film oxides or films with native oxide.

Results: The total SEY can be explained by EUV absorption in the topmost nanometer of (native) oxide of the investigated materials.

Conclusions: Although the relative SEY of Ru and Sn is well-explained by the difference in EUV absorption properties, the SEY of HfO_2 is almost a factor 2 higher than expected. Based on the energy distribution of secondary electrons, this may be related to a lower barrier for secondary electron emission.

© 2019 Society of Photo-Optical Instrumentation Engineers (SPIE) [DOI: 10.1117/1.JMM.18.3.033501]

Keywords: extreme ultraviolet; secondary electron yield; nanoparticle photoresist.

Paper 19040 received May 16, 2019; accepted for publication Aug. 1, 2019; published online Aug. 23, 2019.

1 Introduction

Irradiation of materials with energetic photons, ions, or electrons results in generation of secondary electron emission from the surface. Secondary electron emission is important for devices such as photon counters, plasma display panels, and electron multipliers,[1,2] whereas for plasma devices, secondary electrons can have adverse effects on stable operation.[3,4] Knowledge about the secondary electron emission of materials is, thus, highly relevant for various device applications. In addition, secondary electrons also play an important role in chemical reactions at surfaces. In the x-ray and extreme ultraviolet (EUV) wavelength range (around 13.5 nm), the typical attenuation length of photons in matter is much longer than that of the generated photoelectrons and secondary electrons. Therefore, it is often assumed that secondary electrons play a much more important role in driving chemical reactions as compared to direct photoabsorption processes.[5] Quantitative measurements of secondary electron yields (SEYs) induced by EUV radiation were performed on EUV mirrors and thin films of protective coating materials, most notably Ru, in order to understand the role of secondary electrons in EUV-induced contamination processes.[6]

Although EUV-induced reactions of contaminants on mirrors are mostly undesirable, the process of exposure of photoresist-coated wafers for lithographic patterning requires efficient use of the available EUV power to ensure high throughput in the chip manufacturing process. Since EUV enables printing of features down to 7 nm lateral size, photoresist layers should be relatively thin (on the order of 40 nm) to prevent collapse defects, but should still absorb a sufficiently high fraction of the available light in order to ensure high production throughput.[7–10] In recent years, researchers have, therefore, investigated resists with metal oxide nanoparticles composed of ZrO_2, HfO_2, or SnO_2, which have higher EUV absorption coefficients compared to organic resists. In photoresists of this type, the relatively high EUV absorption in the metal oxides efficiently generates photoelectrons and secondary electrons, which then induce chemical reactions in organic ligands on the particle, thereby inducing the desired chemical modification upon exposure.[9]

Recently, Fallica et al.[8] did a detailed study of the EUV absorption of different photoresists containing metal oxide particles or clusters, using spin-coated resist films on EUV transmissive membranes. In view of the before-mentioned importance of secondary electrons for inducing chemical reactions, the SEY of metal oxides used in resists may also play a role in their sensitivity. In this paper, we present a model study on the SEY and energy distribution of (native) oxide films of Hf and Sn, compared to a Ru thin film as reference material.[6] Measurements of the total SEY versus photon energy show that the SEY of a Ru thin film can be explained by absorption of EUV radiation in the native oxide present on the film. The relative SEY of native SnO_2, as compared to native RuO_2, is well explained by the difference in EUV absorption of both materials. The measured SEY of HfO_2 is, however, almost a factor 2 higher than expected based

*Address all correspondence to Jacobus M. Sturm, E-mail j.m.sturm@utwente.nl

†Present address: Institute of Engineering, Fontys Hogescholen, Eindhoven, The Netherlands

1932-5150/2019/$28.00 © 2019 SPIE

Downloaded From: https://www.spiedigitallibrary.org/journals/Journal-of-Micro/Nanolithography,-MEMS,-and-MOEMS on 01 Oct 2019
Terms of Use: https://www.spiedigitallibrary.org/terms-of-use

on the EUV absorption. This study shows that the SEY of materials may be, along with EUV absorption, an important factor for the sensitivity of EUV photoresists.

2 Experimental

2.1 *Sample Preparation and Precharacterization*

Ru thin films were used as reference for the SEY measurements, since the EUV optical properties of Ru are well known and the SEY has been studied previously.[6] 20-nm Ru films were deposited by direct current magnetron sputtering on a Si wafer substrate. A 20-nm HfO_2 film was deposited by atomic layer deposition (ALD) in a Picosun R200 ALD reactor, using TEMAHf (tetrakis(ethylmethylamido)hafnium(IV)) and ozone as precursors at a growth temperature of 250°C, which gave a growth per cycle of 0.086 nm. As substrate, a Si wafer precoated with 20 nm Mo (deposited by direct current magnetron sputtering) was used. The Mo film has no particular function in the current experiment, but was deposited for other planned experiments on samples from the same batch, for which a good conductive layer below the oxide was required. A native SnO_2 film on Sn was obtained by depositing 20 nm of Sn metal onto a Si wafer piece precoated with 20 nm Mo (from the same batch as used for the HfO_2 sample) with a thermal evaporator. Details on Sn deposition can be found in Ref. 11. The chemical composition of all samples was precharacterized using a Thermo Scientific ThetaProbe x-ray photoelectron spectroscopy (XPS) instrument, employing monochromatic AlK_α radiation (photon energy $h\nu = 1486.7$ eV). All samples could be measured without using a flood gun for charge compensation, indicating that the oxide films were thin enough to prevent significant sample charging. The Hf 4f spectral region of the HfO_2 sample could be fitted with a single doublet with peak position 18.4 eV for the Hf $4f_{7/2}$ peak, which indicates that stoichiometric HfO_2 was produced. Angle-resolved XPS calculations according to the method and attenuation lengths described by Cumpson and Seah[12] indicated that the Ru film had a native RuO_2 thickness of 0.8 nm, whereas the Sn film was covered with about 2 nm of native SnO_2.

2.2 *Secondary Electron Measurements*

EUV-induced SEY was measured at the ID beamline[13] at the metrology light source (MLS) of the Physikalisch-Technische Bundesanstalt, Berlin, Germany. A Scienta R4000 hemispherical electron analyzer, operated at a pass energy of 20 eV, was used for measurements of the kinetic energy distribution of emitted photoelectrons and secondary electrons at three different wavelengths λ of synchrotron light: $\lambda = 18.0$ nm ($h\nu = 68.88$ eV), $\lambda = 13.5$ nm ($h\nu = 91.84$ eV), and $\lambda = 12.0$ nm ($h\nu = 103.33$ eV). For all results shown in this paper, the synchrotron light was incident at an angle of 45 deg relative to the sample surface normal, whereas photoelectrons emitted along the sample surface normal were detected. The typical photon flux applied for these measurements was 1.4×10^{10} s^{-1}, corresponding to a radiation power of 0.21 μW, focused on a spot on the sample of $\sim$1 mm $\times$ 0.015 mm. The instantaneous peak irradiance from a single-bunch pulse from the synchrotron is a factor 1.25 higher than the specified time-averaged radiation power. Typical measurement times of electron spectra were 2 min. In order to check the effect of limited sensitivity and/or analyzer transmission for low-energy secondary electrons, all secondary electron spectra were measured both with the sample grounded and with a negative sample bias between 8.52 and 8.64 V, in order to accelerate electrons toward the detector. The sample bias was checked with a digital volt meter for each measurement. The pressure in the spectrometer system during operation ranged from 5×10^{-10} to 1×10^{-9} mbar. Most dominant residual gas components were water and hydrogen (partial pressures between 1.5×10^{-10} to 3×10^{-10} mbar), whereas C and CO showed an order of magnitude lower partial pressure. SEY spectra measured on the Ru reference sample were repeated to check for possible influence of photoinduced contamination, but no change in SEY caused by previous measurements on the same spot was found.

Quantitative total yield SEY measurements were performed by measuring the sample current (which was on the order of 1 nA) as a function of wavelength of the incident light, which was scanned from 11 to 19 nm (photon energy 111.9 to 65.4 eV), while simultaneously measuring the ring current of the synchrotron. In order to calibrate the ring current against the photon flux incident on the sample, a separate wavelength sweep was performed where the signal of a calibrated EUV photodiode (type SXUV) positioned at the sample position was measured as function of wavelength and ring current. From these characteristics, the SEY was calculated in units of electrons per incident photon. All samples were measured as introduced, no surface cleaning was applied.

3 Results and Discussion

3.1 *Valence Band Spectra*

Figure 1 shows valence band spectra of the Ru thin film with native oxide (RuO_x), Sn film with native SnO_2 oxide (SnO_x), and HfO_2 thin-film (HfO_2) samples measured at 91.84-eV photon energy. The bottom axis displays the measured kinetic energy E_{kin} of the photoelectrons, whereas the top axis displays the calculated binding energy E_b according to $E_b = h\nu - E_{\text{kin}} - \Phi_{\text{an}}$, where Φ_{an} is the calibrated work

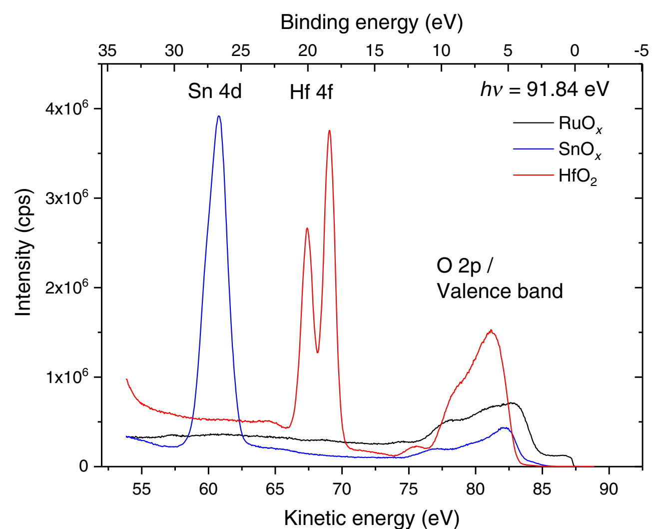

Fig. 1 Valence band spectra of Ru and Sn thin films with native oxide and a HfO_2 thin film measured with 91.84-eV photon energy.

Downloaded From: https://www.spiedigitallibrary.org/journals/Journal-of-Micro/Nanolithography,-MEMS,-and-MOEMS on 01 Oct 2019
Terms of Use: https://www.spiedigitallibrary.org/terms-of-use

function of the analyzer. The RuO_x sample shows metallic characteristics: the Fermi level (or high kinetic energy on-set of the spectrum) is at 0 eV binding energy within the precision of the energy calibration of the analyzer. The metallic characteristics can be assigned to the very small thickness of the native oxide and/or the conductive nature of RuO_2.[14,15] The HfO_2 and SnO_x samples show a band gap: the high-energy on-set of the photoelectron spectrum is significantly below 0 eV binding energy. The measured position of the $Hf4f_{7/2}$ peak in the case of the HfO_2 sample was 18.4 eV, identical to the precharacterization with the laboratory XPS. This shows that possible charging is similar (or absent) as in the reference XPS experiment. Also the Sn 4d level observed for the SnO_x sample was in line with the XPS precharacterization.

3.2 *Secondary Electron Energy Distribution*

Low-energy secondary electron spectra for the three samples, acquired with 91.84 eV photons, are plotted in Fig. 2. Where applicable, the kinetic energy has been corrected for an applied sample bias (used to accelerate electrons toward the analyzer) and a normalized intensity scale is used in order to facilitate comparison of the spectra. When comparing the low energy part of spectra acquired without (a) and with (b) sample bias, the most obvious difference is that measurements with sample bias show a much higher signal of electrons up to about 2.5 eV kinetic energy. This is attributed to limited transmission of the energy analyzer for such low-energy electrons and/or deflection of low-energy electrons by stray magnetic and electric fields in case no accelerating bias is used. In addition, it cannot be excluded that, in the absence of sample bias, the emitted secondary electron flux reduces secondary electron emission due to electrostatic repulsion. This may be an additional reason for a reduced signal of low-energy electrons if no sample bias is used.

In comparison with the Ru film, which only has a thin native oxide, the SnO_x and HfO_2 sample showed a higher total SEY (as shown in Sec. 3.3) and a narrower electron energy distribution with a peak at lower energy. This is in line with previous reports for samples with (native) oxide films and may be attributed to two effects. First, it has been proposed that electron emission causes a positive surface charge. This charge may attract electrons from below the surface and thereby enhance the emission of secondary electrons.[15,16] Alternatively, it has been demonstrated that under conditions for photoelectron emission, downward band bending can occur in (high bandgap) semiconductors, as schematically indicated in Fig. 3(a).[17] This will also lower the barrier for secondary electron emission and make the energy distribution more narrow with a peak at lower kinetic energy.[15] For both the unbiased and biased cases, the kinetic energy of the peak maximum and width of the secondary electron distribution are highest for the RuO_x. However, the kinetic energy peak maximum and width for SnO_x is greater than that for HfO_2 only in the unbiased case. The larger relative shift of the SnO_x peak kinetic energy (and decrease in width) upon application of sample bias, indicates that the barrier for electron emission is more significantly influenced by the application of sample bias, compared to HfO_2. This change of peak maximum and width was consistent for all three photon energies studied. The origin of this effect may be related to the before-mentioned influence of band bending on the barrier for emission of secondary electrons. A negative sample bias applied to the substrate holder will enhance the band bending over the ~2 nm insulating native SnO_x film [see Fig. 3(b)], thereby enhancing the transport of electrons toward the surface and lowering the barrier for emission of secondary electrons. On the contrary, the same substrate bias generates an order of magnitude lower electric field over the HfO_2 layer, which was a 20-nm-thick oxide film. In that case, a negative sample bias thus has a smaller effect on lowering the barrier for secondary electron emission.

Figure 4 shows secondary electron energy distributions for the HfO_2 sample acquired with three different photon energies, both with and without sample bias. The shape of the secondary electron distributions is virtually independent of the photon energy used for excitation, which can be explained by the fact that low-energy secondary electrons are generated by multiple excitations where primary photoelectrons generate secondary electrons that may themselves generate lower energy secondaries. Similarly, no significant

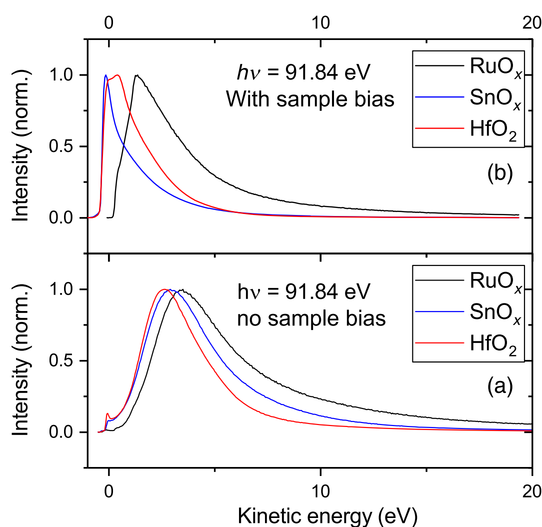

Fig. 2 Measured energy distributions of secondary electrons for illumination with 91.84-eV photon energy (a) without and (b) with sample bias to accelerate electrons toward the energy analyzer. Spectra are normalized to 1 and the energy scale is corrected for the applied sample bias.

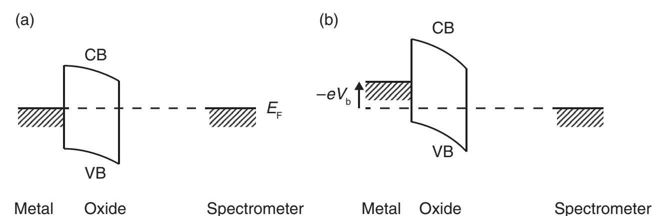

Fig. 3 Schematic band diagram indicating the influence of band bending on secondary electron emission, VB and CB denote valence and conduction bands of the (native) oxide on the sample. (a) Without sample bias, the Fermi level of the metal in the sample aligns with the Fermi level of the spectrometer. Electron emission may lead to positive surface charge on the oxide film, resulting in downward band bending, which lowers the barrier for secondary electron emission.[17] (b) Application of a negative sample bias on the substrate may further enhance this band bending and lower the barrier for SE emission.

Downloaded From: https://www.spiedigitallibrary.org/journals/Journal-of-Micro/Nanolithography,-MEMS,-and-MOEMS on 01 Oct 2019
Terms of Use: https://www.spiedigitallibrary.org/terms-of-use

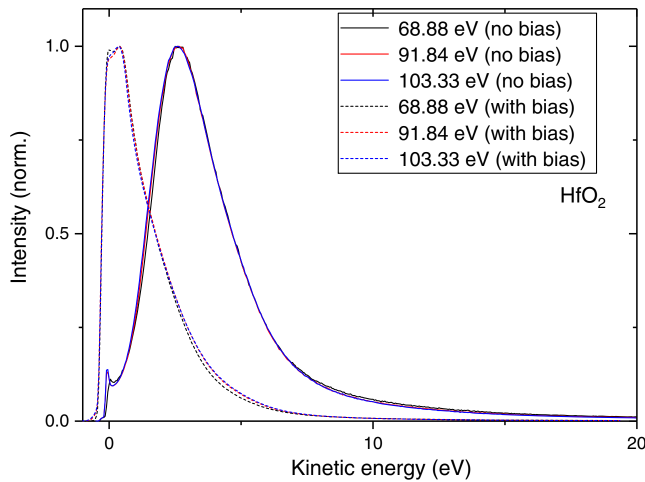

Fig. 4 Energy distribution of secondary electrons from the HfO_2 thin-film sample for different photon energies. Solid lines indicate measurements without sample bias, and dashed lines indicate measurements with bias. Similarly, also for the RuO_x and SnO_x samples, no significant influence of the photon energy on the shape of the energy distribution was found.

influence of the photon energy was found for the secondary electron spectra of RuO_x and SnO_x samples.

3.3 *Quantitative Total Secondary Electron Yields*

Quantitative measurements of the SEY were performed by measuring sample current, without application of sample bias. Figure 5 shows the obtained SEY in electron per photon as a function of photon energy (solid lines). The measured SEY for the RuO_x sample (black line) is in good agreement with previous measurements of Ru with native oxide by Yakshinskiy et al.[6] Within the investigated photon energy range, the SEY drops with increasing photon energy. Since generation of photoelectrons and secondary electrons is the main process by which EUV is absorbed in matter,[5] we investigated whether the energy dependence of EUV

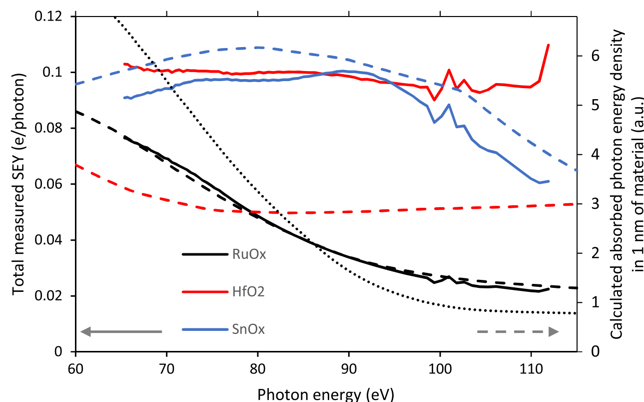

Fig. 5 Total measured SEY versus incident photon energy (continuous lines and left axis) compared to the theoretical dependence of the absorbed photon energy of a 1-nm film of RuO_2, HfO_2, or SnO_2 (dashed lines, right axis) on photon energy. The black dotted line shows the theoretical absorbed photon energy of a 1-nm film of Ru metal. All theoretical curves of absorbed photon energy are scaled with a single scaling factor, such that optimal overlap between the SEY curve of the RuO_x sample and the absorbed photon energy in RuO_2 is obtained.

Table 1 EUV attenuation length ($h\nu = 92$ eV) of materials studied in this research, according to Refs. 18 and 19.

Material	X-ray attenuation length (nm)
Ru	63.7
RuO_2	50.2
Sn	14.9
SnO_2	15.3
HfO_2	31.8

absorption in the sample can explain the measured SEY curve. The attenuation length of the employed synchrotron light, defined as the thickness of material needed to attenuate normally incident light to $1/e$ intensity, ranges from roughly 15 to 64 nm for the materials studied in this work, as outlined in Table 1.[18,19] This means that all investigated thin films absorb only part of the incoming synchrotron light. On the contrary, the attenuation length for low-energy electrons is much shorter. Taking a kinetic energy of 50 eV as reference value, the attenuation length of electrons in RuO_2, HfO_2, and SnO_2 is around 0.25 nm as calculated according to the method of Cumpson and Seah.[12,20] Consequently, it is expected that most of the photoelectrons and secondary electrons emitted from the sample surface will originate from the topmost nm of the sample. We, therefore, compare the measured SEY with the calculated absorbed photon power density in 1 nm of RuO_2, HfO_2, and SnO_2. To this end, the transmission T of 1 nm of these materials is calculated as function of photon energy according to the x-ray absorption data from Henke et al.[18,19] The absorbed photon energy density is then obtained from $h\nu(1-T)$, where $h\nu$ is the photon energy. The absorbed photon energy density for 1-nm RuO_2 is plotted with the dashed black line in Fig. 5, on the right vertical axis. The scale of this axis is adjusted such that an optimal correspondence of the absorbed photon energy with the measured SEY curve is obtained. As can be observed from this figure, the dependence of the SEY on photon energy can be nearly perfectly described by photon absorption in the topmost $\sim$1 nm of RuO_2 on the sample. On the contrary, when the SEY is compared to the absorbed photon energy in 1 nm of Ru metal (black dotted line), no good agreement of the dependence of the SEY on photon energy can be achieved. It is thus unlikely that photon absorption in the Ru metal below the $\sim$0.8 nm native oxide film has a significant influence on the emitted secondary electrons, since in that case one would expect more similarity of the SEY curve to the energy dependence of photon absorption in Ru metal. From this, we conclude that photon absorption in the topmost nm of material is decisive for the emitted secondary electrons, in line with expectations based on the attenuation length of low-energy electrons generated by EUV light.

Subsequently, we compare the SEY of the SnO_x and HfO_2 samples versus photon energy with absorbed photon energy in 1 nm films of SnO_2 and HfO_2. It should be noted that all dashed curves representing absorbed photon energy density are scaled with the same factor as the absorbed photon

Downloaded From: https://www.spiedigitallibrary.org/journals/Journal-of-Micro/Nanolithography,-MEMS,-and-MOEMS on 01 Oct 2019
Terms of Use: https://www.spiedigitallibrary.org/terms-of-use

energy curve for RuO_2. Figure 5 thus provides a direct comparison of the expected SEY based on photon absorption and the actual measured total SEY, using the RuO_x sample as a reference. For the Sn film with native oxide, the photon energy dependence of the SEY roughly follows the expected dependence from the absorbed photon energy, only the SEY is about 10% lower than expected. For the HfO_2 film, the measured SEY is almost a factor 2 higher than expected based on the absorbed photon energy. This high SEY is probably related to a low energy barrier for secondary electron emission from HfO_2, which is consistent with the observed low peak energy and small peak width of the SEY curve without bias in Fig. 2(a).

4 Summary and Conclusions

In this paper, we presented measurements of the SEY and secondary electron energy distribution of thin films of Ru and Sn with native oxide, as well as a stoichiometric HfO_2 film. The shape of the low-energy secondary electron energy distribution up to 20 eV kinetic energy is virtually independent of exact photon energy within the probed range from 69 to 103 eV. This is expected, since these low-energy secondary electrons result from multiple excitations induced by higher energy photoelectrons. The shape and peak position of the energy distribution is material dependent, which is related to differences in the energy barrier for secondary electron emission.[15–17] Photon energy-dependent quantitative measurements of the total SEY show that the SEY of Ru can be explained by photons absorbed in the topmost nanometer of native oxide on top of the thin film. This is a consequence of the short attenuation length of about 0.25 nm for photo- and secondary electrons in the studied energy range, which is roughly an order of magnitude less than the attenuation length of EUV photons. The SEY of Sn with native oxide is well-explained by the higher EUV absorption compared to RuO_2, whereas the total yield of HfO_2 is a factor 2 higher than would be expected based on EUV absorption.

These measurements show that the energy barrier for secondary electron emission is an important factor to consider for processes where secondary electrons can play a decisive role, such as contamination of EUV optical elements and inorganic nanoparticle photoresists. Additionally, the observation that the outermost (few) nm of material appears decisive for the SEY indicates that photoresists with metal oxide nanoparticles, in which secondary electrons generated in the metal oxide induce reactions in organic ligands, will make most efficient use of the available EUV photons when the size of the metal oxide particles is on the order of a few nm.

Acknowledgments

This work is the part of the Industrial Partnership Program "Controlling photon and plasma induced processes at EUV optical surfaces" (CP3E), co-funded by Carl Zeiss SMT, ASML, the Stichting voor Fundamenteel Onderzoek der Materie (FOM), and the Nederlandse Organisatie voor Wetenschappelijk Onderzoek (NWO). The group of Prof. Eberhardt (Berlin) is acknowledged for giving access to instrumentation for electron spectroscopy at the ID beamline. The MLS staff is acknowledged for the technical support during the beam time.

References

1. V. Prodanovic et al., "Effect of thermal annealing and chemical treatments on secondary electron emission properties of atomic layer deposited MgO," *J. Vac. Sci. Technol. A* **36**(6), 06A102 (2018).
2. A. U. Mane et al., "An atomic layer deposition method to fabricate economical and robust large area microchannel plates for photodetectors," *Phys. Procedia* **37**, 722–732 (2012).
3. G. D. Hobbs and J. A. Wesson, "Heat flow through a Langmuir sheath in the presence of electron emission," *Plasma Phys*. **9**(1), 85–87 (1967).
4. M. I. Patino et al., "Analysis of secondary electron emission for conducting materials using 4-grid LEED/AES optics," *J. Phys. D: Appl. Phys.* **48**(19), 195204 (2015).
5. T. E. Madey et al., "Surface phenomena related to mirror degradation in extreme ultraviolet (EUV) litography," *Appl. Surf. Sci.* **253**, 1691–1708 (2006).
6. B. V. Yakshinskiy et al., "Carbon accumulation and mitigation processes, and secondary electron yields of ruthenium surfaces," *Proc. SPIE* **6517**, 65172Z–65171 (2007).
7. M. Kryask et al., "Nanoparticle photoresists: ligand exchange as a new and sensitive EUV patterning mechanism," *J. Photopolym. Sci. Technol.* **26**(5), 659–664 (2013).
8. R. Fallica et al., "Absorption coefficient of metal-containing photoresists in the extreme ultraviolet," *J. Micro/Nanolithogr. MEMS MOEMS* **17**(2), 023505 (2018).
9. S. Chakrabarty et al., "Oxide nanoparticle EUV resists: toward understanding the mechanism of positive and negative tone patterning," *Proc. SPIE* **8679**, 867906 (2013).
10. H. Xu et al., "EUV photolithography: resist progress in metal-organic complex photoresists," *J. Micro/Nanolithogr. MEMS MOEMS* **18**(1), 011007 (2019).
11. M. Pachecka et al., "Electronegativity-dependent tin etching from thin films," *AIP Adv.* **6**(7), 075222 (2016).
12. P. J. Cumpson and M. P. Seah, "Elastic scattering corrections in AES and XPS. II. Estimating attenuation lengths and conditions required for their valid use in overlayer/substrate experiments," *Surf. Interface Anal.* **25**(6), 430–446 (1997).
13. A. Gottwald, H. Kaser, and M. Kolbe, "The U125 insertion device beamline at the metrology light source," *J. Synchrotron Radiat.* **26**, 535–542 (2019).
14. L. Krusin-Elbaum and M. Wittmer, "Conducting transition-metal oxides—possibilities for RUO2 in VLSI metallization," *J. Electrochem. Soc.* **135**(10), 2610–2614 (1988).
15. S. Iida et al., "An analysis of the impact of native oxide, surface contamination and material density on total electron yield in the absence of surface charging effects," *Appl. Surf. Sci.* **384**, 244–250 (2016).
16. L. Malter, "Thin film field emission," *Phys. Rev.* **50**(1), 48–58 (1936).
17. C. Bandis and B. B. Pate, "Photoelectric emission from negative-electron-affinity diamond (111) surfaces: exciton breakup versus conduction-band emission," *Phys. Rev. B* **52**(16), 12056–12071 (1995).
18. B. L. Henke et al., "X-Ray interactions with matter," http://henke.lbl.gov/optical_constants/ (1995–2010).
19. B. L. Henke, E. M. Gullikson, and J. C. Davis, "X-Ray interactions—photoabsorption, scattering, transmission, and reflection at $E = 50$–30, 000 ev, $Z = 1$–92," *At. Data Nucl. Data Tables* **54**(2), 181–342 (1993).
20. Thermo Fisher Scientific, *Thermo Avantage Software*, ThermoFisher Scientific, East Grinstead (1999–2018).

Jacobus M. Sturm received his MSc degree from Eindhoven University of Technology in 2001 and his PhD from the University of Twente in 2006. Currently, he is an assistant professor in the XUV Optics Group at the University of Twente. His research mainly involves surface and thin-film analysis related to coatings for extreme UV optics.

Feng Liu conducted research for his PhD in the XUV Optics Group. His research focused on photochemistry of water induced by extreme UV radiation.

Erik Darlatt finished studies of chemistry focused on surface science in 2009 at the University of Leipzig. He started his PhD at the Federal Institute of Material Research Testing in cooperation with the Freie Universität in Berlin. From 2013 to 2017, he had a postdoctoral position at Physikalisch-Technische Bundesanstalt (PTB). Since 2017, he has been working for Carl Zeiss AG, Oberkochen, Germany.

Michael Kolbe received his diploma degree in physics and PhD from the Martin-Luther-University, Halle, Germany, in 1998 and 2002, respectively. Since 2003, he has been a scientist at Germany's National Metrology Institute of the PTB. His current work includes

Downloaded From: https://www.spiedigitallibrary.org/journals/Journal-of-Micro/Nanolithography,-MEMS,-and-MOEMS on 01 Oct 2019
Terms of Use: https://www.spiedigitallibrary.org/terms-of-use

synchrotron radiation-based analytical (spectroscopic, scattering, as well as reflecting) techniques for innovative materials and systems.

Antonius A. I. Aarnink is a senior process engineer in the Integrated Devices and Systems Group at the University of Twente. His current work involves, among others, development of equipment and processes for atomic layer deposition.

Christopher J. Lee obtained his PhD from the University of Otago in 1998. His research interests include nonlinear optics, surface science, and the development of new sensors for health applications. He currently works in the Electrical Engineering Department at Fontys University of Applied Sciences.

Fred Bijkerk received a PhD in experimental physics from the University of Amsterdam in 1993. From 2004 to 2014, he was the department head at the FOM-Institute for Plasma Physics Rijnhuizen. In 2005, he was appointed as a professor on XUV sources and multilayer optics at the University of Twente. He initiated the Industrial Focus Group XUV Optics at MESA+, a public-privately funded research initiative on thin-film systems and XUV optics.

Downloaded From: https://www.spiedigitallibrary.org/journals/Journal-of-Micro/Nanolithography,-MEMS,-and-MOEMS on 01 Oct 2019
Terms of Use: https://www.spiedigitallibrary.org/terms-of-use